Flow Acceleration and Mountain Drag*

PETER R. BANNON

Department of the Geophysical Sciences, The University of Chicago, Chicago, IL 60637

(Manuscript received 2 January 1985, in final form 28 May 1985)

ABSTRACT

Dynamic explanations of mountain drag usually invoke viscous effects and/or wave momentum flux by either Rossby or internal gravity waves. This paper explores an alternative mechanism in terms of the unsteadiness of the incident flow. The reaction to acceleration (local time rate of change) of the flow past a stationary obstacle can manifest itself as a contribution to the drag on the flow.

A simple model provides an estimate of this acceleration reaction in a geophysically relevant context. The shallow-water flow of a periodic current around a right-circular cylinder is determined for subinertial periods and arbitrary rotational Froude number. The results of this prototype calculation support the hypothesis that acceleration reaction may provide a substantial contribution to the mountain drag exerted by mesoscale and synoptic-scale obstacles.

1. Introduction

A ubiquitous feature of atmospheric flow over orography is the asymmetry in the surface pressure field. Typically there is high pressure upstream of the mountain and low pressure in the lee. This pressure gradient implies that the atmosphere is tending to push the mountain downstream. By Newton's third law, the mountain exerts a force on the flow directed upstream. This phenomenon of mountain drag is a particular case of "form" or "pressure" drag in fluid mechanics. Sawyer (1959), Newton (1971), and Lilly (1972) emphasize the synoptic and climatological importance of mountain drag.

The total force, $\mathbf{F}_T$ exerted on an obstacle by fluid stresses acting across a surface S is

$$\mathbf{F}_T = -\int_S p\mathbf{n}dA + \int_S \underline{\tau}\cdot\mathbf{n}dA \qquad (1.1)$$

where p is the fluid pressure, $\underline{\tau}$ is the viscous stress tensor, $\mathbf{n}$ is the unit vector normal to the surface directed toward the fluid, and dA is an elemental area of the surface. The total drag, D_T, on the obstacle is defined as the component of $\mathbf{F}_T$ in the direction opposite to that of mean flow of the fluid, $\mathbf{U}$:

$$D_T \equiv \mathbf{U}\cdot\mathbf{F}_T = -\int_S p\mathbf{U}\cdot\mathbf{n}dA + \int_S \mathbf{U}\cdot\underline{\tau}\cdot\mathbf{n}dA \qquad (1.2)$$

where $\mathbf{U}$ is a constant unit vector. [Here we use a coordinate system in which the bounding surface (mountain) is at rest.] The second term on the right-hand side of (1.2) is the direct contribution to the drag due to the viscous stress. It is usually called the surface friction, skin friction or wall friction and depends on the distribution of tangential shear stress over the surface. In contrast, the mountain drag is the first term in (1.2) and depends on the distribution of the pressure over the surface.

Various processes have been proposed to explain the occurrence of mountain drag (see Table 1). They may be categorized using d'Alembert's (1752) paradox, of which a modern statement is: Steady inviscid adiabatic flow generates no drag on a finite obstacle in the absence of waves. A common but restrictive assumption is that the atmospheric flow is steady. By making this assumption one is led by d'Alembert's paradox to conclude that the mountain drag is the result of (i) viscous effects, (ii) wave momentum flux, and/or (iii) diabatic processes.

In addition to generating a surface friction contribution to the total drag, viscosity can alter the pressure pattern associated with the flow and thus affect the mountain drag. In quasi-geostrophic flow, for example, Ekman pumping has been shown (e.g., Vaziri and Boyer, 1971; Buzzi and Tibaldi, 1977) to generate significant mountain drag. In this case the appropriate inverse Reynolds number is the ratio $\sqrt{E}/\epsilon$, where E is the Ekman number and ϵ is the Rossby number. (The notation follows Pedlosky, 1979, with the horizontal length scale of the flow taken to be the mountain half-width a.) Typically, $\sqrt{E} < 10^{-1}$ in the atmosphere. For synoptic-scale mountains of order $a \approx 10^3$ km, the Rossby number is small, $\epsilon \approx 10^{-1}$, so the effects of Ekman pumping are not negligible. However, for mesoscale mountains, ($a \approx 10^2$ km), $\epsilon \approx 1$, and the effects should be less important. For smaller mountains, (a

* Results presented at the First Conference on Mesoscale Meteorology in Norman, Oklahoma, 31 May–3 June 1983.

TABLE 1. Mechanisms of mountain drag.

Mechanism	Process
Viscosity	Flow separation Ekman pumping
Wave Propagation	Buoyancy waves Rossby waves
Heating	Surface flux of heat and moisture Latent heat release Radiative heating
Flow Unsteadiness	Acceleration reaction

$<$ 10 km), Ekman pumping is insignificant, but flow separation associated with viscous effects could possibly produce a significant aerodynamic drag (Smith, 1978) in the lee of sharp peaks. It is important to note that although Ekman pumping and flow separation are physically distinct processes, both are produced by viscosity.

An exception to the preceding remark is inviscid flows with free-streamline discontinuities that start at the point of separation on the obstacle and extend downstream to infinity. A stagnant wake can then exist behind the obstacle, and a drag is present. Kirchhoff's (e.g., Lamb, 1945; see Sections 73–79, 370) flow around a flat plate aligned normal to the incident flow is one example. Such solutions are unstable however. Inclusion of the caveat that d'Alembert's paradox holds for flows, all of whose steamlines exist upstream, precludes this class and refines the statement of the paradox given above.

Stationary waves excited by the mountain can produce mountain drag by their ability to propagate energy and momentum away from the obstacle. On the synoptic scale, Rossby waves can produce a significant mountain drag for westerly flow (e.g., Janowitz, 1977). On the mesoscale and smaller, Rossby wave excitation is usually ignored. [The horizontal scale, $(U/\beta)^{1/2}/2\pi$, of the lee trough associated with the beta effect is large compared to observations for mesoscale obstacles, and an asymmetry between eastward and westward flow is not evident.]

Mountain drag can also be generated by internal gravity waves. The drag due to these buoyancy waves decreases, however, as rotation increases (Smith, 1979). Smith (1982) has presented this argument for mesoscale mountains. While qualitative agreement with many flow features is attained, the magnitude of the surface pressure distribution is underestimated for mesoscale mountain ranges.

Important diabatic processes in the atmosphere include sensible heat flux from the surface, radiative heating, and the latent-heat release of precipitation. Of these, the first two act relatively slowly (i.e., on time scales of days) and hence could have significant effects for synoptic-scale mountains, (e.g., a mountain separating two air mass source regions). In contrast, latent-heat release is fast acting and can be important on all time scales. Analytic and numerical studies (Barcilon *et al.*, 1979, 1980; Durran, 1981) indicate that by reducing the static stability of the atmosphere, moisture and precipitation reduces the mountain drag for small ($L \approx 10$ km) mountain ridges. Similar studies for mesoscale and synoptic-scale mountains are not available in the literature.

Each of these mechanisms for mountain drag can operate in a steady state. It is the purpose of this investigation to explore an additional mechanism in terms of the unsteadiness of the incident flow. In unsteady flow, the pressure distribution at a given instant differs from that for the corresponding steady velocity distribution because an additional force is required for acceleration or deceleration. This dynamic imbalance can manifest itself as a pressure drag.

A crude estimate of this acceleration reaction can be obtained from potential flow theory of classical fluid dynamics. In a homogeneous, inviscid, infinite fluid, the drag exerted on a body by the accelerating flow field is (e.g., Batchelor, 1967)

$$D_A = \alpha \rho V \frac{\partial U}{\partial t}, \tag{1.3}$$

where ρ is the fluid density, V the volume of the body, and $\partial U/\partial t$ is the flow acceleration. Here α is the coefficient of virtual inertia and depends only on the shape of the body. Typically, $\alpha = O(1)$, being unity for a circular cylinder and one-half for a sphere. That the potential flow solution is solely a function of the geometry implies that the energy of the moving fluid is completely determined by the instantaneous motion of the flow relative to the body. Such a simplification is not necessarily valid in a geophysical flow. Buoyancy and inertia waves may be present, and α is no longer just a geometric factor but depends also on the stratification and rotation. Nonetheless the model results presented below provide some *a posteriori* justification of the estimate (1.3) for the geophysical case.

For comparison the mountain wave drag for steady flow over a ridge with a profile of the form $h_m = h(1 + x^2/a^2)^{-1}$ is $D_W \leqslant \pi \rho N U h^2 L/4$ (Smith, 1979) where N is the buoyancy frequency, h the mountain height, a the mountain width, L the mountain length, and the inequality holds for rotating flow. Thus one measure of the relative importance of the acceleration reaction is

$$\frac{D_A}{D_W} \geqslant \frac{4\alpha a}{N \tau_A h}, \tag{1.4}$$

where τ_A is a characteristic acceleration time. With $\alpha = 1$, $a = 100$ km, $N = 10^{-2}$ s^{-1}, and $h = 1$ km, the acceleration and wave drags are of comparable magnitude for $\tau_A \approx 0.5$ day. This comparison suggests that acceleration drag may be relatively large for obstacles whose width is greater than 100 km.

Traditional arguments for ignoring transient effects in flow over mountains are based on the assumption of a small Strouhal number S. Here S is defined as the ratio of the local to advective acceleration

$$S = \left|\frac{\partial u/\partial t}{u \cdot \nabla u}\right| = \frac{a}{U\tau_A} \tag{1.5}$$

where U is a flow speed ($\approx$10 m/s) and τ_A the flow acceleration time. Flow transience is assumed small if $S \ll 1$. For an isolated mesoscale mountain peak (e.g., $a < 10$ km), it can be ignored if $\tau_A \gg 10^3$ s. However, for a mountain massif (e.g., $a \approx 10^3$ km), the criterion is $\tau_A \gg 10^5$ s. The transience of observed synoptic-scale flows may therefore be important for large mountain ranges but not for an isolated mountain.

In the presence of waves the importance of transience depends on the time, τ_W, required for the establishment of the wave pattern over the domain. Roughly $\tau_W = L/c_g$ where L is a characteristic scale of the domain and c_g the characteristic wave group velocity. Then τ_W would replace the advective time a/U in (1.5). Since $c_g \geqslant U$ but $L \gg a$ typically, (1.5) may underestimate the importance of transience.

The next section develops a simple model to illustrate the effects of flow unsteadiness on mountain drag. A basic assumption is that all the incident flow goes around rather than over the topographic feature. Blocking or damming of low-level flow by orography is commonly observed (e.g., by the Alps, Appalachians, East African highlands, and South African escarpment; see Sections 4 and 5). By explicitly ignoring the effects of viscosity, wave momentum flux and diabatic processes, the model isolates the role of the flow acceleration in generating mountain drag. As such the model is viewed as a prototype. The inclusion of more physical processes will undoubtedly improve the realism of the model, but the goal here is rather to derive a simple estimate of acceleration drag in a geophysically relevant context. It is in this spirit that the model is developed in Section 2. Results deduced from the model are described in Section 3. The paper concludes with a discussion of these results and their relevance to atmospheric situations.

2. The model

The model is specifically designed to examine mean flow acceleration as a mechanism for mountain drag. It consists of two inviscid fluid layers of constant density ρ and ρ' in hydrostatic balance on an f-plane. The depth of the upper layer is taken to be large compared to the depth, h, of the lower layer. Thus motions excited aloft will be small and are ignored. The presence of the upper layer, however, introduces a reduced gravity $g' = g(\rho - \rho')/\rho$ reflecting the stable stratification. Here ρ' and ρ are the fluid densities in the upper and lower layer, respectively.

An isolated mountain lies at the center of a Cartesian coordinate system (x, y, z). The mountain shape is a right circular cylinder of a radius a and height h_m described by the equation

$$\xi = z - h_m[1 - H(r - a)] = 0, \tag{2.1}$$

where H is the Heaviside step function and $r^2 = x^2 + y^2$. Here $h_m > h$; this assumption precludes the intersection of the interface with the mountain top. Apart from this constraint, the mountain height is arbitrary. Figure 1 summarizes the model geometry; the usual meteorological notation holds.

Far from the obstacle the flow is zonal, spatially uniform and periodic in time so that

$$\lim_{r\to\infty} \mathbf{u}(x, y, z, t) = U \exp(-i\omega t)\mathbf{i}. \tag{2.2}$$

This forcing is assumed to be weak so that linear theory holds. By (1.5), this assumption restricts attention to flows of large Strouhal number S. Physically this restriction requires that fluid parcels travel a distance small compared to the mountain width before the flow reversals. Nonlinear effects are discussed *a posteriori*. Then in (2.2) and all subsequent complex equations, the real part is assumed. Attention is restricted to synoptic time scales such that $\omega < |f|$ so that no radially propagating waves are allowed.

The above assumptions eliminate viscous effects, wave momentum flux and diabatic processes as causes of any mountain drag realized by the model. Hence the model is viewed as a prototype for an estimate of acceleration drag in a meteorological context.

The governing equations of motion and of continuity for the model are therefore the linear shallow water equations

$$\frac{\partial u}{\partial t} - fv = -g'\frac{\partial \eta}{\partial x} + X, \tag{2.3a}$$

$$\frac{\partial v}{\partial t} + fu = -g'\frac{\partial \eta}{\partial y}, \tag{2.3b}$$

$$\frac{\partial \eta}{\partial t} + h\left(\frac{\partial u}{\partial x} + \frac{\partial v}{\partial y}\right) = Q, \tag{2.3c}$$

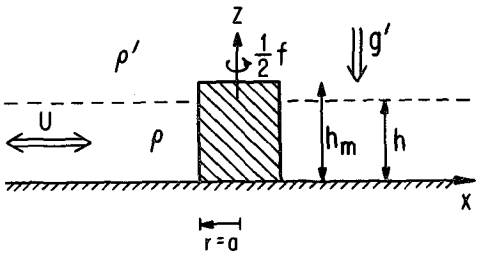

FIG. 1. Schematic illustration of the model. The atmosphere is a two-layer fluid (with reduced gravity g') on an f-plane. A periodic zonal current with amplitude U and frequency ω is incident on a circular cylinder of radius a and height h_m.

where η is the deviation of the fluid interface from its mean position. Because the incident flow is periodic in time, the linearization is about a state of rest.

A body force, X, in the zonal direction and a mass source–sink term, Q, are included in the x-momentum equation (2.3a) and continuity (2.3c), respectively. Physically X may arise from a pressure gradient force imposed on the lower by the upper layer or from the net effect of bottom and interfacial stresses acting on the depth-averaged flow (e.g., Gill, 1982, Section 9.9) or from horizontal Reynolds stress divergence. The term Q is often interpreted as a heating term (e.g., Matsuno, 1966). These prescribed forcing terms are introduced as a formal means of driving the incident flow. Their presence in (2.3) and their exact form [see (2.5)] are not crucial to the results of the analysis, nor is their detailed physical justification essential to the present investigation. The thrust of this paper is the interaction of a given incident flow with the model orography and not with the generation of the flow. Given the fact that time varying zonal flow can be generated in a manner consistent with the governing equations (2.3), attention may then be focused on the interaction of the flow with the topography.

For the incident flow (2.2), the set (2.3) becomes, assuming solutions of the form $\exp(-i\omega t)$,

$$-i\omega u = X, \tag{2.4a}$$

$$+fu = -g' \frac{\partial \eta}{\partial y}, \tag{2.4b}$$

$$-i\omega\eta = Q. \tag{2.4c}$$

The solution is an oscillating zonal flow in geostrophic balance:

$$u_I = U \exp(-i\omega t), \tag{2.5a}$$

$$\eta_I = -\frac{Ufy}{g'} \exp(-i\omega t), \tag{2.5b}$$

$$X = -i\omega U \exp(-i\omega t), \tag{2.5c}$$

$$Q = \frac{i\omega Ufy}{g'} \exp(-i\omega t), \tag{2.5d}$$

where the subscript I denotes the solution in the absence of the mountains.

With the mountain present, the total solution is the sum of the incident and scattered components, for example

$$\mathbf{u} = \mathbf{u}_I + \mathbf{u}_S, \tag{2.6}$$

where $\mathbf{u}_S$ is the solution to the homogeneous form of (2.3) subject to the inhomogeneous kinematic boundary condition

$$(\mathbf{u}_I + \mathbf{u}_S)\cdot\mathbf{r} = 0 \quad \text{at} \quad r = a, \tag{2.7}$$

where $\mathbf{r}$ is the unit radial vector in cylindrical coordinates (r, θ). The scattered pressure field $p_S = \rho g' \eta_S$ satisfies

$$\nabla^2 p_S = \frac{f^2 - \omega^2}{g'h} p_S, \tag{2.8}$$

which has the solution in cylindrical coordinates

$$p_S = \rho Ufai \exp(-i\omega t) \times \sum_{m=-\infty}^{+\infty} \exp(im\theta)[C_m K_m(\lambda r) + D_m I_m(\lambda r)] \tag{2.9}$$

where $\lambda^2 = (f^2 - \omega^2)/g'h$ and K_m and I_m are modified Bessel functions (e.g., Abramowitz and Stegun, 1974) such that $K_{-m}(Z) = K_m(Z)$; $I_{-m}(Z) = I_m(Z)$. The factor $\rho Ufai$ is introduced for convenience. As the I_m are unbounded as $r \to \infty$, setting $D_m = 0$ ensures a bounded solution.

The C_m are determined from the boundary condition (2.7). The scattered velocity fields are

$$\mathbf{u}_S\cdot\mathbf{r} = \frac{1}{\rho(f^2 - \omega^2)}\left[i\omega \frac{\partial p_S}{\partial r} - \frac{f}{r}\frac{\partial p_S}{\partial \theta}\right], \tag{2.10a}$$

$$\mathbf{u}_S\cdot\theta = \frac{1}{\rho(f^2 - \omega^2)}\left[f\frac{\partial p_S}{\partial r} + \frac{i\omega}{r}\frac{\partial p_S}{\partial \theta}\right], \tag{2.10b}$$

while

$$\mathbf{u}_I\cdot\mathbf{r} = U\exp(-i\omega t)\cos\theta = \frac{U}{2}\exp(-i\omega t)[\exp(i\theta) + \exp(-i\theta)]. \tag{2.11}$$

By the orthogonality of the $\exp(im\theta)$, it is found

$$C_m = 0 \quad \text{for} \quad |m| \neq 1, \tag{2.12}$$

and

$$C_{\pm 1} = \frac{(1 - \sigma^2)/2}{\left[\dfrac{a\sigma\partial K_1(\lambda r)}{\partial r}\bigg|_{r=a} \mp K_1(\lambda a)\right]}, \tag{2.13}$$

where $\sigma = \omega/f$ or, upon evaluating the derivative,

$$C_{\pm 1} = \frac{(1 - \sigma^2)}{\{-\sigma\lambda a[K_0(\lambda a) + K_2(\lambda a)] \mp 2K_1(\lambda a)\}}, \tag{2.14}$$

Thus the scattered pressure field is

$$p_S = \rho Ufai \exp(-i\omega t)[C_1 \exp(i\theta) + C_{-1}\exp(-i\theta)]K_1(\lambda r). \tag{2.15}$$

3. Results

The flow response, (2.15) with (2.14), to the presence of the mountains has many interesting features. Figure 2 provides an example for the case where the nondimensional frequency $\sigma = 0.50$ and the rotational Froude number $F = f^2a^2/g'h = 1$. First we note that the response is trapped next to the obstacle. The modified Bessel function has the asymptotic forms

$$K_1(Z) \approx \frac{1}{Z} \quad \text{for} \quad Z \ll 1, \tag{3.1}$$

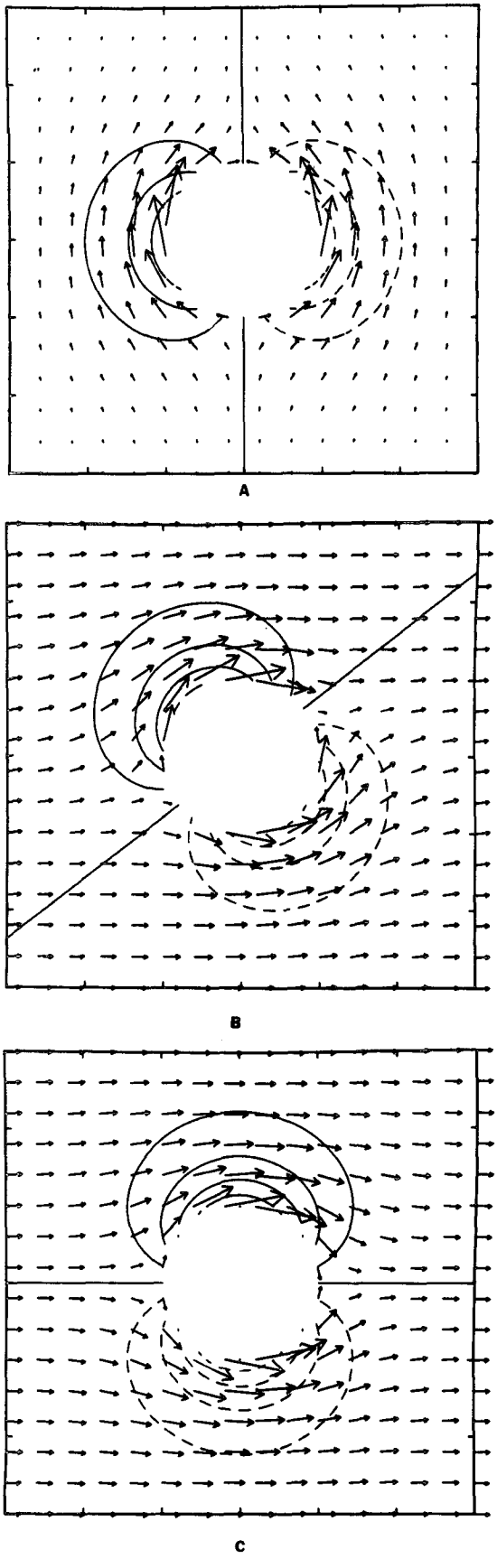

and

$$K_1(Z) \approx \left(\frac{\pi}{2Z}\right)^{1/2} e^{-Z} \quad \text{for} \quad Z \gg 1. \tag{3.2}$$

The characteristic decay distance is $\lambda^{-1} = \{g'h/[f^2(1 - \sigma^2)]\}^{1/2}$ and is proportional to the Rossby radius of deformation. This radial structure is a consequence of the fact that (2.8) prohibits any radially propagating solution for subinertial ($\omega < f$) frequencies.

Note that for low frequencies ($\sigma < 1$), F is approximately the square of the ratio of the mountain scale a to the decay distance λ^{-1}. In such cases, the solution exhibits exponential decay [see (3.2)], and a boundary layer structure with barrier trapped winds for small F. For large F the decay follows (3.1) and there is a potential flow regime. Pierrehumbert and Wyman (1985) make a similar argument based on nonlinear continuously stratified numerical calculations. (See their Fig. 19 and discussion.)

In addition the pressure response exhibits a high–low pressure distribution across the cylinder. This dipole pattern propagates clockwise around the cylinder (f is assumed >0), and its magnitude varies in time. Mathematically the solution consists of both a clockwise and counterclockwise mode. The dominance of the former arises because the denominator in (2.14) is smaller for $m = -1$ than $m = +1$. Resonance occurs when σ and F are such that the denominator vanishes. This situation corresponds to the free mode of the system with $m = -1$ and $\mathbf{u}_S \cdot \mathbf{r} = 0$ at $r = a$. The free modes have been calculated by Longuet-Higgins (1969); they are Kelvin waves modified by curvature effects. No free modes with $m > 0$ exist.

The total force acting on the fluid by the mountain is

$$\mathbf{F} = \int p \nabla \xi dx dy, \tag{3.3}$$

where $p = p_I + p_S = pg'\eta$, and ξ is given by (2.1). By symmetry $\mathbf{F} \cdot \mathbf{k} = F_z = 0$. The forces in the x and y directions are found to be

$$F_x = \rho VUfi \exp(-i\omega t)\hat{P}_x, \tag{3.4a}$$

$$F_y = \rho VUf \exp(-i\omega t)(\hat{P}_y - 1), \tag{3.4b}$$

where $V = \pi a^2 h$ is the volume of the cylinder, and $\hat{P}_x$ and $\hat{P}_y$ are nondimensional pressure coefficients

$$\hat{P}_x = (C_1 + C_{-1})K_1(\lambda a), \tag{3.5a}$$

$$\hat{P}_y = (C_{-1} - C_1)K_1(\lambda a). \tag{3.5b}$$

FIG. 2. Time sequence of the scattered pressure field and total velocity field for nondimensional frequency $\sigma = \omega/f = 0.5$ and rotational Froude number $F = f^2a^2/g'h = 1$. The circular void at the center corresponds to the cylindrical mountain of unit radius. The pressure contour interval is $0.4\rho Ufa$ with negative contours dashed. The speed of the largest velocity vector is (1.9, 3.1, 4.0) U for frames (a), (b) and (c), respectively. (a) $\omega t = -\pi/2$; (b) $\omega t = -\pi/4$; (c) $\omega t = 0$.

Note that $|\hat{P}_x|$ and $|\hat{P}_y|$ give the magnitude of the scaled pressure at $r = a$ on the x and y axis, respectively. The incident pressure field p_I contributes the factor of unity in (3.4b) but makes no contribution to (3.4a). For the case illustrated in Fig. 2, where $\sigma = 0.50$ and $F = 1$, $\hat{P}_x = 1.58$ and $\hat{P}_y = 2.00$.

The phase of the response is such that the maximum east–west pressure difference occurs at $\omega t = \pi/2$ and $3\pi/2$. High pressure is found upwind of the obstacle a quarter period ahead of the far-field flow u_I. Thus the drag on the flow is in phase with the far-field acceleration $\partial u_I/\partial t$ but leads u_I by a quarter period. In contrast the north–south pressure difference is a maximum at $\omega t = 0$ and π. The lift $(-F_y)$ on the obstacle is 180° out of phase with u_I and leads the far-field acceleration by a quarter period. It should be noted that direct application of these phase results of drag and lift to real atmospheric flows can be difficult since the flow acceleration is often not parallel to the flow.

The quasi-geostrophic result (which requires $U/fa \ll 1$) is obtained by taking the limit as $(\omega/f) \to 0$ with f fixed. The result is

$$p_S = \rho U f a \sin\theta \cos\omega t K_1[\sqrt{F}(r/a)]/K_1(\sqrt{F}). \quad (3.6)$$

Unlike the steady, nonlinear case (e.g., Merkine and Solan, 1979), this linear, transient solution feels the effect of the free surface. In the limit as $F \to 0$ (i.e., a rigid lid), (3.6) reduces to

$$p_S = \rho U f a \sin\theta \cos\omega t (a/r) \quad (3.7)$$

which, apart from the factor $\cos(\omega t)$, is identical to the steady nonlinear result and to that for potential theory. The effect of the free surface is to increase the trapping of the response. A plot of (3.6) for $F = 1$ (Fig. 3) shows

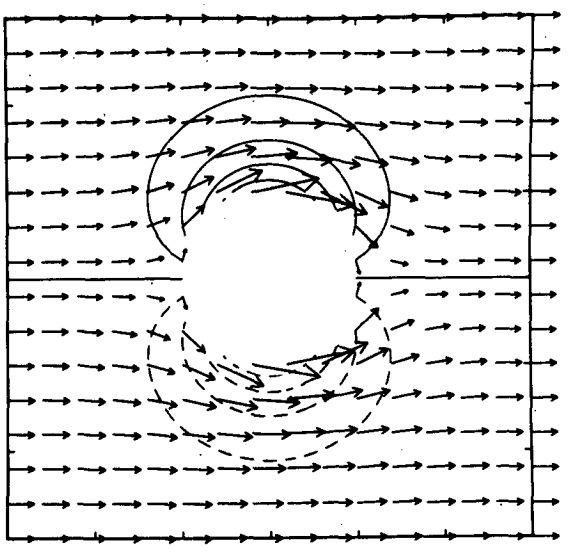

FIG. 3. As in Fig. 2 but for the quasi-geostrophic case: $\sigma \ll 1$ and $F = 1$. The fields are shown here at $t = 0$; they are modulated by the factor $\cos\omega t$. The contour interval is $0.2\rho Ufa$ and the speed of the largest velocity vector is $2.6U$.

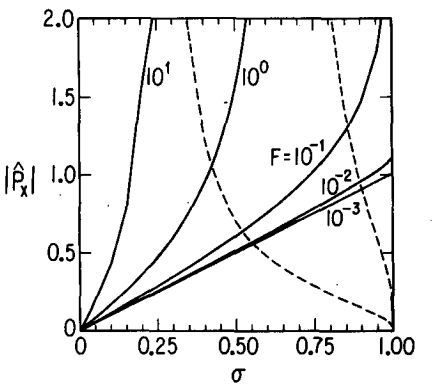

FIG. 4. The magnitude of $\hat{P}_x$ given by (3.5a) plotted as a function of $\sigma = \omega/f$ for various values of F. $\hat{P}_x$ is positive (negative) on the solid (dashed) curve. $\hat{P}_x$ is a measure of the east–west pressure gradient across the mountain and the mountain "drag."

a stationary dipole response that oscillates in time. In the quasi-geostrophic case, the clockwise and counterclockwise modes are equally excited ($C_{-1} = -C_{+1}$), and there is no north–south asymmetry of the flow. [Note, however, that the $\sigma = 0$ solution is degenerate in the sense that an arbitrary radially symmetric ($m = 0$) component that vanishes in the far field can be added to the solution.] Furthermore $\hat{P}_x = 0$ and $\hat{P}_y = 1$; there is neither drag nor lift.

The highly ageostrophic nature of the earlier result (Fig. 2) is revealed by comparison with Fig. 3. The ageostrophy leads to a stronger, asymmetric propagating response with both a drag and lift.

Both flow patterns exhibit strong splitting of the incident flow. The tangential velocities are supergeostrophic $|u_\theta| \leqslant 2.59U$ for $m = -1$ and subgeostrophic $|u_\theta| \leqslant 0.58U$ for $m = +1$. In the geostrophic case $|u_\theta| \leqslant 0.85U$ for $m = \pm 1$. These strong, topographically trapped, tangential velocities are reminiscent of mountain winds such as the bise and the mistral. Pierrehumbert and Wyman (1985) also found topographically trapped barrier winds.

The model results for a variety of parameter settings are compactly summarized in Figs. 4 and 5, which provide plots of $\hat{P}_x$ and $\hat{P}_y$ as a function of σ for various values of F. [Inspection of (2.14) indicates that $\hat{P}_x$ and $\hat{P}_y$ are functions of σ and F only.] In Fig. 4, $\hat{P}_x$ has two zeros at $\sigma = 0$ and 1. The first is a statement of d'Alembert's paradox; it also corresponds to the quasi-geostrophic result. The second zero corresponds to a forced inertial oscillation with $p_S = 0$. (The special case $\omega = f$ is treated in the Appendix.) For a given F, $\hat{P}_x$ is infinite at $\sigma = \sigma_R$ where resonance with the free $m = -1$ mode of Longuet-Higgins occurs. As Figs. 4 and 5 indicate, $\sigma_R \propto 1/F$ and $\sigma_R \approx 1$ for $F < 10$, $\sigma_R = 0.275$ (0.680) for $F = 10$ (1).

Figure 5 displays similar plots for $\hat{P}_y$. At $\sigma = 0$, $\hat{P}_y = 1$ and the total sideways force $F_y = 0$. At $\sigma = 1$, $\hat{P}_y = 0$; but $F_y = 0$ as the incident pressure field p_I contributes to the lift. The resonance peaks occur at the same σ_R as in Fig. 4.

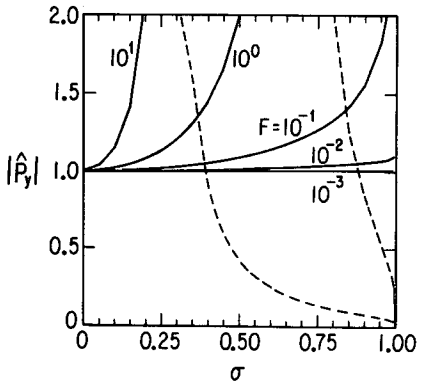

FIG. 5. The magnitude of $\hat{P}_y$ given by (3.5b) plotted as a function of $\sigma = \omega/f$ for various values of F. $\hat{P}_y$ is positive (negative) on the solid (dashed) curves. $1 - \hat{P}_y$ is a measure of the north–south pressure gradient across the mountain and the "lift" on the mountain.

In addition to being resonance frequencies, the σ_R also denote transition points in the flow response. For $\sigma > \sigma_R$, the sign of the coefficient C_{-1} reverses from its $\sigma < \sigma_R$ value. The coefficient C_{+1} suffers no sign reversal. Since $|C_{-1}| > |C_{+1}|$ for all nonzero σ, this sign change implies a reversal in the phase of the response. For example, the drag on the fluid is 180° out of phase with the acceleration for $\sigma > \sigma_R$.

The preceding results for drag and lift should be compared to the potential flow result of (1.3) with $\alpha = 1$ for a cylinder. In such a case, $\hat{P}_x = \sigma$ and $\hat{P}_y = 0$; there is no resonance or phase reversal. In the present stratified rotating model, the coefficient of virtual inertia, α, is a tensor whose elements are functions of σ and F and are often greater than unity in magnitude.

4. Discussion

The prototype model of acceleration reaction in a geophysical context presented here consists of a linear analysis of the periodic flow of an inviscid, rotating, shallow-water, fluid around a cylinder. In the model a cross-mountain pressure drag arises solely due to the unsteadiness of the flow incident on the mountain.

The major results of the calculations are summarized in Figs. 4 and 5, which plot $\hat{P}_x$ and $\hat{P}_y$, respectively, as a function of the nondimensional frequency $\sigma = \omega/f$ for various rotational Froude numbers $F = f^2a^2/g'h$. Here $\hat{P}_x$ and $\hat{P}_y$ denote the maximum scaled (by the factor ρUfa) pressure response at $r = a$ in the x and y direction. By (3.4), $\hat{P}_x$ and $1 - \hat{P}_y$ alternatively represent the scaled magnitude of the drag and lift forces. Here the drag and lift are assigned directions relative to that of the acceleration that in general will not correspond to the flow direction.

Application of these results to the atmosphere requires a choice of the depth scale h and the reduced gravity g'. In some cases low-level inversions motivate a two-layer model of the atmosphere, and then h is the inversion height and g' reflects the inversion strength. Examples of this approach include Gill (1977) in the case of coastal lows and Bannon (1979) in the case of the East African jet. For a continuously stratified fluid, these choices are not clear-cut. As noted previously, however, the model results for the barotropic case exhibit features (e.g., barrier winds trapped within a deformation radius of the obstacle) similar to those of Pierrehumbert and Wyman (1985) for a continuously stratified fluid. This comparison suggests equating the Froude number F to that for the continuous case $f^2a^2/N^2h_m^2$.

Proceeding in this manner for the typical atmospheric values of $f = 10^{-4}$ s^{-1}, $h = 3$ km, $N = 10^{-2}$ s^{-1}, $g' = N^2h = 0.30$ m s^{-2}, one finds the rotating Froude number: $F = 10^{-3}$, 10^{-1} and 10 for $a = 10$, 100 and 1000 km, respectively. Inspection of Figs. 4 and 5 reveals that acceleration drag and lift are more significant for large mountains. This preference is reinforced by the fact that the scaling for the pressure and drag varies linearly and quadratically with the mountain radius a. Taking $\sigma = 0.50$ and $U = 5$ m s^{-1}, the Strouhal number $S = \omega a/U$ for these mountain widths is 10^{-1}, 10^0, and 10, respectively. Thus the linear assumption is not unreasonable for the larger mountain. The model predicts maximum pressure differences of

$$\left.\begin{aligned} \Delta p_x &\equiv 2\rho Ufa|\hat{P}_x| = 4.7 \text{ mb} \\ \Delta p_y &\equiv 2\rho Ufa[|\hat{P}_y| - 1] = 3.0 \text{ mb} \end{aligned}\right\}, \tag{4.1}$$

for $a = 300$ km ($F = 1$, $S = 3$, $U/fa = \frac{1}{6}$). In contrast, the steady linear lee wave analysis of Smith (1982) predicts $\Delta p_x = 1.14$ mb and $\Delta p_y = 0$ for the same parameter settings. It should be noted that the pressure gradient is orthogonal to the flow at the time of maximum wind. This result is not consistent with typical observations over the Alps.

The magnitude of the model drag is comparable to that predicted by wave processes. Inspection of (1.2), (1.3) and (3.4a) indicates that the coefficient of virtual inertia $\alpha = (f/\omega)\hat{P}_x$ is O(1), thus supporting the comparison of the acceleration reaction with the linear mountain wave drag made in the Introduction. A similar comparison with the Rossby wave drag ($D_R \leq (\rho f^2V^2/2\pi H)(\beta/U)^{1/2}$ where $H = 10$ km is the tropopause height; see Janowitz, 1977) leads to

$$\frac{D_A}{D_R} \geqslant \frac{2\pi\alpha HU}{\tau_A f^2 V}(U/\beta)^{1/2}.$$

Taking $\alpha = 1$, $U = 10$ m s^{-1}, $\beta = 2 \times 10^{-11}$ m^{-1} s^{-1}, $f = 10^{-4}$ s^{-1}, $h = 1$ km and $a = 10^3$ km, the acceleration and Rossby wave drags are comparable for $\tau_A \approx 0.2$ day. These model results lend support to the hypothesis that the acceleration reaction may contribute significantly to the mountain drag exhibited over mesoscale and synoptic-scale orographic features.

It is worthwhile to note that the predicted acceleration reaction (3.4a) has a zero time mean. This result is a consequence of the use of a periodic incident flow

but suggests that the acceleration drag would make no direct contribution to the mean flow in a climatological sense.

At a given instant, however, the drag is present and can act on the flow. In the linear model developed here, this feedback is precluded since the temporal variation of the zonal flow is prescribed. In the real atmosphere, however, the drag may act and affect the subsequent time evolution of a synoptic event. Furthermore the results suggest caution in the interpretation of high–low pressure patterns over orography present in individual synoptic charts; such patterns may not necessarily arise solely from either viscous, wave or diabatic processes or from their combination.

The analysis is restricted to a periodically changing zonal flow that is horizontally homogeneous. Fourier analysis techniques would enable the solution for arbitrary time dependence to be calculated by superposition. In addition it is straightforward to allow for spatial variation in the incident flow. For a spatially varying u_I, the scattered wave is again given by (2.9) with $D_m = 0$. But now monopole ($m = 0$) and quadrupole ($|m| > 2$) contributions to the pressure field will be present. However, by symmetry, only the dipole ($|m| = 1$) terms contribute to the drag and lift forces.

An important simplifying assumption is the use of the linear model equations. The solution (2.5) for the incident flow is an exact solution to the fully nonlinear set of equations. Close to the obstacle the total radial component of flow becomes vanishingly small by the kinematic condition (2.7); hence radial advective accelerations will be small there. Tangential accelerations, however, can be significant and will produce a nonlinear steepening of the flow. Gill (1977) has modeled this steepening process in a ridge geometry for the coastal low of South Africa. Curvature effects are small for synoptic-scale mountains but increase in importance for mesoscale and smaller mountains.

5. Conclusion

The goal of this study has been to demonstrate that temporal dependence of the incident flow can, by itself, lead to the production of a high–low pressure asymmetry across a mountain and hence produce a mountain drag. The present work provides a barotropic model of this phenomenon. Examples of mountain drag associated with transient flow in a continuously stratified fluid are also present in the literature. In the numerical solution of Huppert and Bryan (1976, Figs. 5, 8, 10–11), dipole density anomalies across a mountain are predicted for a flow that has been impulsively started from rest. The drag implied by these anomalies arises in part from the transience of the flow since the steady state solutions (e.g., Johnson, 1978a,b) for such bound vortex pairs exhibit no drag. (The small lateral viscosity may also contribute to the creation of a drag. Surface friction is absent in the simulation.) Analytic studies for impulsively started, inviscid quasi-geostrophic flow over topography also display a drag (Bannon, 1983, Section 4b) in the absence of Rossby waves.

Baines (1980) provides some observational support for an acceleration reaction. The time evolution of a cold front interacting with the mountains of southwest Australia produces coastally trapped gravity currents and a deformation of the surface isobars. Similar pressure deformations associated with cold fronts are depicted in Buzzi and Tibaldi (1977, Fig. 5) for the Alps and in Smith (1982, Fig. 5) for New Zealand.

Future research should focus on the assessment of acceleration reaction in more realistic models with a mean background wind and continuous stratification and on observational case studies.

Acknowledgments. I benefitted from general discussion with Professor George W. Platzman on drag and the forces on bodies moving through a fluid and from his review of an early version of the manuscript. Professor Dave Fultz brought the class of free-streamline discontinuous solutions to my attention. Reviewer A made numerous insightful and constructive comments on the manuscript. Financial support was provided jointly by the National Science Foundation and the National Oceanic and Atmospheric Administration under grants ATM 80-26790 and ATM 84-02249 and by the Louis Block Fund of the University of Chicago. The numerical computations were performed on the CDC 7600 of the National Center for Atmospheric Research, which is sponsored by the National Science Foundation.

APPENDIX

The Case $\omega = f$

For solutions proportional to $\exp(-ift)$, the homogeneous form of (2.3) in cylindrical coordinates is

$$-ifu_r - fu_\theta = -g' \frac{\partial \eta}{\partial r}, \tag{A1}$$

$$-ifu_\theta + fu_r = \frac{-g'}{r} \frac{\partial \eta}{\partial \theta}, \tag{A2}$$

$$-if\eta + h\left[\frac{1}{r}\frac{\partial}{\partial r}(ru_r) + \frac{1}{r}\frac{\partial u_\theta}{\partial \theta}\right] = 0. \tag{A3}$$

Solving (A1) for u_θ yields

$$u_\theta = -iu_r + \frac{g'}{f}\frac{\partial \eta}{\partial r} \tag{A4}$$

and substituting into (A2) one finds that η satisfies

$$-i\frac{\partial \eta}{\partial r} + \frac{1}{r}\frac{\partial \eta}{\partial \theta} = 0, \tag{A5}$$

which has the general solution

$$\eta = \sum_{m=-\infty}^{+\infty} A_m \exp(im\theta) r^m \exp(-ift). \tag{A6}$$

The radial component of velocity satisfies

$$\frac{1}{r}\frac{\partial(ru_r)}{\partial r} - \frac{i}{r}\frac{\partial u_r}{\partial \theta} = \frac{if\eta}{h} - \frac{g'}{rf}\frac{\partial^2 \eta}{\partial r \partial \theta}, \tag{A7}$$

which is derived by substituting (A4) into (A3). It is straightforward to show that (A7) with η given by (A6) has the solution

$$u_r = \sum_{m=-\infty}^{+\infty} \frac{if}{h} A_m \exp(im\theta) B_m(r) \exp(-ift) + \sum_{n=-\infty}^{+\infty} E_n \exp(in\theta) r^{-(n+1)} \exp(-ift), \tag{A8}$$

where the first series is the particular solution and the second is the homogeneous solution. The radial functions $B_m(r)$ are

$$B_m(r) = \begin{cases} a_m r^{m+1} + b_m r^{m-1}, & m \neq 0, -1 \\ a_0 r - \dfrac{g'h}{f^2 r} \ln r, & m = 0 \\ \ln r + b_{-1} r^{-2}, & m = -1, \end{cases} \tag{A9}$$

where

$$\left.\begin{aligned} 2(m+1)a_m &= 1 \\ 2mb_m &= -g'h/f^2 \end{aligned}\right\}. \tag{A10}$$

An expression for the tangential component of velocity can be obtained by substituting (A6) and (A8) into (A4).

The constants A_m and E_n are determined from the boundary conditions. For solutions bounded as $r \to \infty$, one requires that $A_m = 0$ for $m \geqslant -1$ and that $E_n = 0$ for $n \leqslant -2$. The remaining constants are determined from the kinematic boundary condition (2.7). The particular solution in (A8) vanishes. Thus the solution when $\omega = f$ is

$$u_r = \frac{U}{2} \exp(-ift)\left[\frac{a^2}{r^2}\exp(i\theta) + \exp(-i\theta)\right], \tag{A11}$$

with $\eta = 0$ and $u_\theta = -iu_r$. The solution is not a function of F. The scattered velocity field is finite at $r = \infty$ and (2.2) is not satisfied. The obstacle has an influence upstream.

REFERENCES

Abramowitz, M., and I. A. Stegun, 1974: *Handbook of Mathematical Functions.* National Bureau of Standards, 1046 pp.

Baines, P. G., 1980: The dynamics of the southerly burster. *Aust. Meteor. Mag.*, **28,** 175–200.

Bannon, P. R., 1979: On the dynamics of the East African jet. Part I: Simulation of mean conditions for July. *J. Atmos. Sci.*, **36,** 2139–2152.

——, 1983: Quasi-geostrophic frontogenesis over topography. *J. Atmos. Sci.*, **40,** 2266–2277.

Barcilon, A., J. C. Jusem and P. G. Drazin, 1979: On the two-dimensional hydrostatic flow of a stream of moist air over a mountain ridge. *Geophys. Astrophys. Fluid Dyn.*, **13,** 125–140.

——, —— and S. Blumsack, 1980: Pseudoadiabatic flow over a two-dimensional ridge. *Geophys. Astrophys. Fluid Dyn.*, **16,** 19–33.

Batchelor, G. K., 1967: *An Introduction to Fluid Dynamics.* Cambridge University Press, 615 pp.

Buzzi, A., and S. Tibaldi, 1977: Inertial and frictional effects on rotating stratified flow over topography. *Quart. J. Roy. Meteor. Soc.*, **103,** 135–150.

d'Alembert, J., 1752: *Essai d'une Nouvelle Theorie de la Resistance des Fluides.* David l'aine, 212 pp. [Reprinted 1966 Bruxelles: Culture et Civilisation. An English translation of the relevant section appears in Dugas (1955).]

Dugas, R., 1955: *A History of Mechanics.* Trans. J. R. Maddox, Griffon, 671 pp.

Durran, D. R., 1981: The effects of moisture on mountain lee waves. Ph.D. thesis, Massachusetts Institute of Technology, 142 pp. [NTIS PB82156621.]

Gill, A. E., 1977: Coastally trapped waves in the atmosphere. *Quart. J. Roy. Meteor. Soc.*, **103,** 431–440.

——, 1982: *Atmosphere-Ocean Dynamics.* Academic Press, 662 pages.

Huppert, H. E., and K. Bryan, 1976: Topographically generated eddies. *Deep-Sea Res.*, **23,** 655–679.

Janowitz, G. S., 1977: The barotropic Rossby wave drag due to an isolated topography. *J. Atmos. Sci.*, **34,** 802–805.

Johnson, E. R., 1978a: Topographically bound vortices. *Geophys. Astrophys. Fluid Dyn.*, **11,** 61–71.

——, 1978b: Trapped vortices in rotating flow. *J. Fluid Mech.*, **86,** 209–224.

Lamb, H., 1945: *Hydrodynamics.* Dover, 738 pp.

Lilly, D. K., 1972: Wave momentum flux—a GARP problem. *Bull. Amer. Meteor. Soc.*, **53,** 17–23.

Longuet-Higgins, M. S., 1969: On the trapping of long-period waves round islands. *J. Fluid Mech.*, **37,** 773–784.

Matsuno, T., 1966: Quasi-geostrophic motions in the equatorial area. *J. Meteor. Soc. Japan,* **44,** 25–42.

Merkine, L.-O., and A. Solan, 1979: The separation of flow past a cylinder in a rotating system. *J. Fluid Mech.*, **92,** 381–392.

Newton, C. W., 1971: Mountain torques in the global angular momentum balance. *J. Atmos. Sci.*, **28,** 623–628.

Pedlosky, J., 1979: *Geophysical Fluid Dynamics.* Springer-Verlag, 624 pp.

Pierrehumbert, R. T., and B. Wyman, 1985: Upstream effects of mesoscale mountains. *J. Atmos. Sci.*, **42,** 977–1003.

Sawyer, J. S., 1959: The introduction of the effects of topography into methods of numerical forecasting. *Quart. J. Roy. Meteor. Soc.*, **85,** 31–43.

Smith, R. B., 1978: A measurement of mountain drag. *J. Atmos. Sci.*, **35,** 1644–1654.

——, 1979: The influence of the earth's rotation on mountain wave drag. *J. Atmos. Sci.*, **36,** 177–180.

——, 1982: Synoptic observations and theory of orographically disturbed wind and pressure. *J. Atmos. Sci.*, **39,** 60–70.

Vaziri, A., and D. L. Boyer, 1971: Rotating flow over shallow topographies. *J. Fluid Mech.*, **50,** 79–95.